



# Negative ion formation through dissociative electron attachment to Germanium tetrachloride

Baldur Brynjarsson



Faculty of Physical Sciences  
University of Iceland  
2014

**Negative ion formation through  
dissociative electron attachment  
to Germanium tetrachloride**

Baldur Brynjarsson

15 ECTS thesis submitted in partial fulfillment of a  
*Baccalaureus Scientiarum* degree in Chemistry

Advisor  
Oddur Ingólfsson

Faculty of Physical Sciences  
School of Engineering and Natural Sciences  
University of Iceland  
Reykjavik, May 2014

Negative ion formation through  
dissociative electron attachment  
to Germanium tetrachloride

15 ECTS thesis submitted in partial fulfillment of a B.Sc. degree in Chemistry

Copyright © 2014 Baldur Brynjarsson  
All rights reserved

Faculty of Physical Sciences  
School of Engineering and Natural Sciences  
University of Iceland  
VRII, Hjarðarhagi 2-6  
107, Reykjavík  
Iceland  
Telephone: 525 4000

Bibliographic information:

Baldur Brynjarsson, 2014, Negative ion formation through  
dissociative electron attachment  
to Germanium tetrachloride, B.Sc. thesis, Faculty of Physical Sciences, University of Iceland.

Printing: Háskólaprent, Fálkagata 2, 107 Reykjavík  
Reykjavík, Iceland, May 2014

# Acknowledgements

First and foremost, I would like to thank my supervisor, Professor Oddur Ingólfsson for the opportunity to take on a Bachelor assignment. Furthermore, I thank him for the very helpful and instructive editing process, his input improved this thesis greatly.

The work presented in this thesis was done in collaboration with a fantastic research group: Benni, Frímann, Ragesh, Rachel, Stefán, Birkir and Ragnheiður all contributed to this work in some way and for that I thank them deeply. It's been a fantastic spring semester.

I would like to especially thank two of the group members, Dr. Benedikt Ómarsson and Dr. Frímann Haukur Ómarsson. Their patience knows no limits and the help and input they provided was instrumental during the course of the thesis work.

Additionally, I thank one particular group member, Stefán Kristinsson, who has accompanied me throughout all three years of my studies and partnered with me on countless assignments.

Finally, I would like to thank my family for their love, warmth and support throughout the course of my life. Their encouragement has brought me to where I am today and for that I am eternally grateful. To all my friends I give special thanks for the good times that were had when I probably should have been writing this thesis.

# Abstract

The interaction of low-energy electrons with neutral gaseous molecules can provide important information about various processes observed in atmospheric chemistry, plasma industry, fiber optics and many more. Low-energy electron interaction with molecules is governed by the formation of a transient negative ion (TNI) which is bound to relax subsequently. One of the relaxation pathways leads to the dissociation of the molecule and formation of a negative fragment. This process is termed Dissociative Electron Attachment (DEA) and is the main focus of the present study.

$\text{GeCl}_4$  is used extensively in the production of fiber optic materials as well as in other industries where low-energy electrons can play an important role. As a part of an effort to characterize the interaction of low-energy electrons with the group IV tetrahalides  $\text{XY}_4$  ( $\text{X} = \text{C}, \text{Si}, \text{Ge}$  and  $\text{Y} = \text{F}, \text{Cl}, \text{Br}$ ), dissociative electron attachment to  $\text{GeCl}_4$  in the incident electron energy range from  $\sim 0$  to 10 eV is presented and discussed in context with previous studies. The Appearance Energy (AE) of contributions in the ion yield is determined by fitting the onset of ion yield curve with functions that reproduce the onset. In this study, two independent fitting functions were used, a Wannier type function and a linear function.

The observed fragments from the current DEA measurements were  $\text{GeCl}_3^-$ ,  $\text{GeCl}_2^-$ ,  $\text{Cl}_2^-$  and  $\text{Cl}^-$ . These fragments were formed through three resonances which appeared in the ion yields at  $\sim 0$ , 1.4 and 5-6 eV and have been assigned to  $\text{A}_1$ ,  $\text{T}_2$  and E symmetries, respectively. The presented measurements provide ion yields with higher resolution than has been obtained before and whereas the results were mostly in agreement with earlier studies, a few features were observed for the first time. In the  $\text{GeCl}_3^-$  yield, all three resonances were observed together in one spectra. At 0 eV, the formation of  $\text{GeCl}_3^-$  dominates the ion yield due to the high electron affinity of  $\text{GeCl}_3^-$ , making it the energetically favorable pathway. However, through the higher energy resonance at 5-6 eV, the formation of  $\text{Cl}^-$  is the preferred pathway. This might be due to increased probability density of the electron around the chlorine atom in the transient negative ion.

# Útdráttur

Víxlverkun lágorkurafeinda við óhlaðnar sameindir á gasformi gegnir veigamiklu hlutverki á ýmsum sviðum, til að mynda í efnafræði andrúmsloftsins, í rafgösum, við framleiðslu ljósleiðara og á fleiri sviðum. Þessi víxlverkun einkennist af myndun neikvætt hlaðinna jóna (móðurjóna) sem alla jafna eru í örvuðu ástandi og leitast því við að losna við þá umframorku sem þær tók upp í myndunarferlinu. Móðurjónirnar geta aförvast með rofi efnatengja, við það myndast eitt eða fleiri stöðug óhlaðin sameindabrot og eitt stöðugt hlaðið sameindabrot. Þetta ferli nefnist rjúfandi rafeindarálagning (e. Dissociative Electron Attachment; DEA) og er meginviðfangsefni þessarrar ritgerðar.

Þessi rannsókn er hluti af stærra verkefni sem miðar að því að kortleggja víxlverkun lágorkurafeinda við tetrahalíð frumefna úr IV flokki lotukerfisins  $XY_4$  ( $X = C, Si, Ge$  og  $Y = F, Cl, Br$ ). Þessi efni eru mikið notuð í iðnaði og framleiðsluferlum þar sem lágorkurafeindir gegna mikilvægu hlutverki. Í þessari rannsókn var rjúfandi rafeindarálagning á Germaníum tetraklóríð ( $GeCl_4$ ) á bilinu  $\sim 0$  til 10 eV skoðuð og niðurstöður ræddar í samhengi við aðrar rannsóknir sem gerðar hafa verið á sama efni. Auk þess var það orkugildi, þar sem fyrst gætir myndunar stöðugar jónar (e. Appearance Energy), ákvarðað með notkun sniðfalla. Notaðar voru tvær ólíkar gerðir sniðfalla, annarsvegar veldisfall af Wannier gerð og hinsvegar línulegt fall.

Þau hlöðnu sameindabrot sem mynduðust við rjúfandi rafeindarálagningu á  $GeCl_4$  voru  $GeCl_3^-$ ,  $GeCl_2^-$ ,  $Cl_2^-$  og  $Cl^-$ . Þessi sameindabrot urðu til við niðurbrot móðurjóna sem mynduðust við 0, 1.4 og 5-6 eV. Sýnt hefur verið að samhverfu móðurjónanna sé best lýst með ókjúfanlegu framsetningunum  $A_1$ ,  $T_2$  og  $E$ . Hægt var í þessu verkefni að ákvarða nakvæmar þau orkugildi þar sem þessi sameindabrott myndast og þótt flestar niðurstöður séu í samræmi við fyrri rannsóknir, sáust nokkur einkenni sem ekki hafa sést áður. Til að mynda sást  $GeCl_3^-$  jónin myndast við öll þrjú orkugildin. Auk þess sást  $Cl^-$  jónin myndast við 0 eV, en möguleiki á myndun hennar við 0 eV hafði áður verið dregin í efa. Við leiðum líkur að því að ríkjandi myndun  $GeCl_3^-$  við 0 eV sé vegna hárrar rafeindasækni jónarinnar. Hins vegar er ríkjandi myndun  $Cl^-$  jónarinnar við 5-6 eV líklega sökum þess að við þessa orku er rafeindin staðsett meira í námunda við klóratómið.

# Contents

Acknowledgements	i
<b>1 Introduction</b>	<b>1</b>
<b>2 Theoretical Overview</b>	<b>4</b>
2.1 Negative ion formation and decay . . . . .	4
2.2 Negative ion resonances . . . . .	6
<b>3 Methods</b>	<b>9</b>
3.1 Experimental setup . . . . .	9
3.2 Energy Calibration . . . . .	10
3.3 Determination of Appearance Energy . . . . .	12
<b>4 Results And Discussion</b>	<b>13</b>
4.1 Positive ion mass scan . . . . .	14
4.2 Determination of the appearance energy . . . . .	15
4.3 Dissociative electron attachment to $\text{GeCl}_4$ . . . . .	17
4.3.1 Ion yield at around 0 eV . . . . .	19
4.3.2 Ion yield at around 1.4 eV . . . . .	21
4.3.3 Ion yield in the range of 4-7 eV . . . . .	21
<b>5 Summary</b>	<b>23</b>
<b>List of Figures</b>	<b>24</b>
<b>List of Tables</b>	<b>24</b>
<b>Bibliography</b>	<b>25</b>

# 1 Introduction

This study is a contribution to an effort to characterize electron attachment reactions to the group IV tetrahalides,  $XY_4$  ( $X = C, Si, Ge$  and  $Y = F, Cl, Br$ ), while simultaneously summarizing available literature on low-energy electron interactions with these compounds. Previously, the group IV tetrafluorides<sup>1</sup> and tetrabromides<sup>2</sup> have been studied and articles were subsequently published in the International Journal of Mass Spectrometry. The results and literature summary of this thesis will serve as a part of an upcoming article on the group IV tetrachlorides.

The study of low-energy electron interaction with  $GeCl_4$  is both of fundamental and practical interest. Although  $GeCl_4$  has limited industrial use in and of itself, it is extensively used as an intermediate in the production of germanium dioxide and purified germanium metal. Germanium dioxide,  $GeO_2$ , is principally used for fiber optics,<sup>3</sup> infrared optics, and as a polymerization catalyst<sup>4</sup> as well as for electronic and solar applications.<sup>5</sup> Due to its excellent refractive properties, it can also be used in synchrotron X-ray diffraction<sup>6</sup> and gamma-ray spectroscopy,<sup>7</sup> which is instrumental in the search for dark matter. High purity germanium can be used as an alloying agent; for example, adding germanium to a bronze alloy has been shown to improve its corrosion resistance and a small germanium content in sterling silver has been found to improve resistance to tarnish and firestain damages.<sup>8</sup>

In the field of low-energy electron interaction research,  $GeCl_4$  has been broadly studied, including various experimental and theoretical methods. In addition to the previous group IV tetrahalides,<sup>1,2</sup> the results from the current measurements will be compared to two main studies: by Pabst *et al.* in 1977<sup>9</sup> and Guillot *et al.* in 1996.<sup>10</sup> Pabst *et al.*<sup>9</sup> focused on DEA to the tetrachlorides and -bromides of silicon and germanium. For  $GeCl_4$ , they observed two resonances yielding  $GeCl_3^-$ ,  $GeCl_2^-$ ,  $Cl_2^-$  and  $Cl^-$  anions and determined the electron affinity of the first two ions as well as estimating their kinetic energy. However, the study only covers resonances that appear for electron energy above 1 eV and therefore does not disclose any information on the threshold region. Guillot *et al.*<sup>10</sup> published an extensive study on empty levels in a few germanium compounds, including  $GeCl_4$ , using X-ray Absorption Spectroscopy (XAS), inner shell electron energy loss spectroscopy (ISEELS), *ab initio* calculations, Electron Transmission Spectroscopy (ETS) and Dissociative Electron Attachment (DEA). Two resonances were observed at 0 and 5-6 eV through their contributions to the DEA ion yields of  $GeCl_3^-$ ,  $Cl^-$  and  $GeCl_2^-$ ; out of which the formation of  $Cl^-$  dominated at

## 1 Introduction

5 eV. The electron transmission spectrum also revealed two resonant states located at 1.7 and 5.6 eV. These resonances were assigned  $T_2$  and E. While the  $T_2$  resonance was not observed through DEA measurements by Guillot *et al.*<sup>10</sup>, the E resonance was detected through contributions to the  $\text{GeCl}_2^-$  and  $\text{Cl}^-$  ion yields. The absence of  $T_2$  in the DEA measurements was attributed to auto-detachment dominance. Further analysis of these articles and comparison with current results will be presented in chapter 4. In a later study, Modelli *et al.*<sup>11</sup> revisited this topic and extended the study by Guillot *et al.*<sup>10</sup> with bound-state MS-X $\alpha$  calculations. These calculations suggested that  $\text{GeCl}_4$  possesses positive electron affinity in agreement with earlier studies. Their calculated energy of the  $t_2$  orbital also closely matches with the resonances seen by Guillot *et al.*<sup>10</sup> Furthermore, Modelli *et al.*<sup>11</sup> points out an error made by Guillot *et al.*<sup>10</sup> in the interpretation of the intensity of measured  $\text{Cl}^-$  signal in DEA, which lead to an overestimation of the fragments intensity by a factor of 10.

In addition to these DEA studies, an experimental study on the cross section for electron collision with  $\text{GeCl}_4$ , done by Szmytkowski *et al.*,<sup>12</sup> found a sharp increase in the total cross section centered near 1.7 eV. A second broader peak was recorded at 10 eV with a noticeable shoulder around 6 eV. *Ab initio* calculations on the inelastic and elastic integral cross sections of  $\text{GeCl}_4$  were carried out by Azevedo *et al.*<sup>13</sup> These calculations were followed by a computational study on the elastic cross sections of group IV tetrahalides by Mozekjo *et al.*<sup>14</sup> using Independent Atom Model (IAM) calculations.

Other studies relevant to low-energy electron interactions and the electronic structure, but not discussed further in this thesis, include the following studies: A thorough review of gas-phase ion-chemistry of simple germanium systems,<sup>15</sup>  $\text{GeCl}_4$  emission spectra resulting from electron impact,<sup>16</sup> a comparative theoretical study on the structure and energies of the  $\text{GeCl}_3\cdot$  radical,<sup>17</sup> a dissociative multiple photoionization study<sup>18</sup> as well as a study on non-radiative decay pathways by synchrotron radiation.<sup>19</sup>

$\text{GeCl}_4$  has tetrahedral symmetry and thus belongs to the  $T_d$  symmetry group. The determination of the exact electronic structure of  $\text{GeCl}_4$  is important in understanding and assigning symmetry to resonances seen in DEA and ETS. The ordering of valence occupied orbitals for  $\text{GeCl}_4$  has been studied with photoelectron spectroscopy<sup>20,21</sup> and is, in order of increasing energy:  $(8a_1)^2(9t_2)^6(3e)^4(10t_2)^6(2t_1)^6$ . Using X-ray absorption spectra, supported by *ab initio* calculations, Guillot *et al.*<sup>10</sup> found that the lowest unoccupied valence orbitals were, in order of increasing energy,  $(9a_1)(11t_2)(4e)(12t_2)$ . These results were combined into a molecular orbital diagram in the article and to elucidate these results it has been adapted and is presented here (see figure 1.1). Guillot *et al.* later extended their XAS study of the inner shell excitation spectra of  $\text{GeCl}_4$  and observed a linear correlation between (M–Cl) equilibrium bond length (with M = Ge, Sn, P, As) and the energy of the  $\text{Cl } 1s \rightarrow \sigma^*(\text{M–Cl})$  shape resonance.

## 1 Introduction

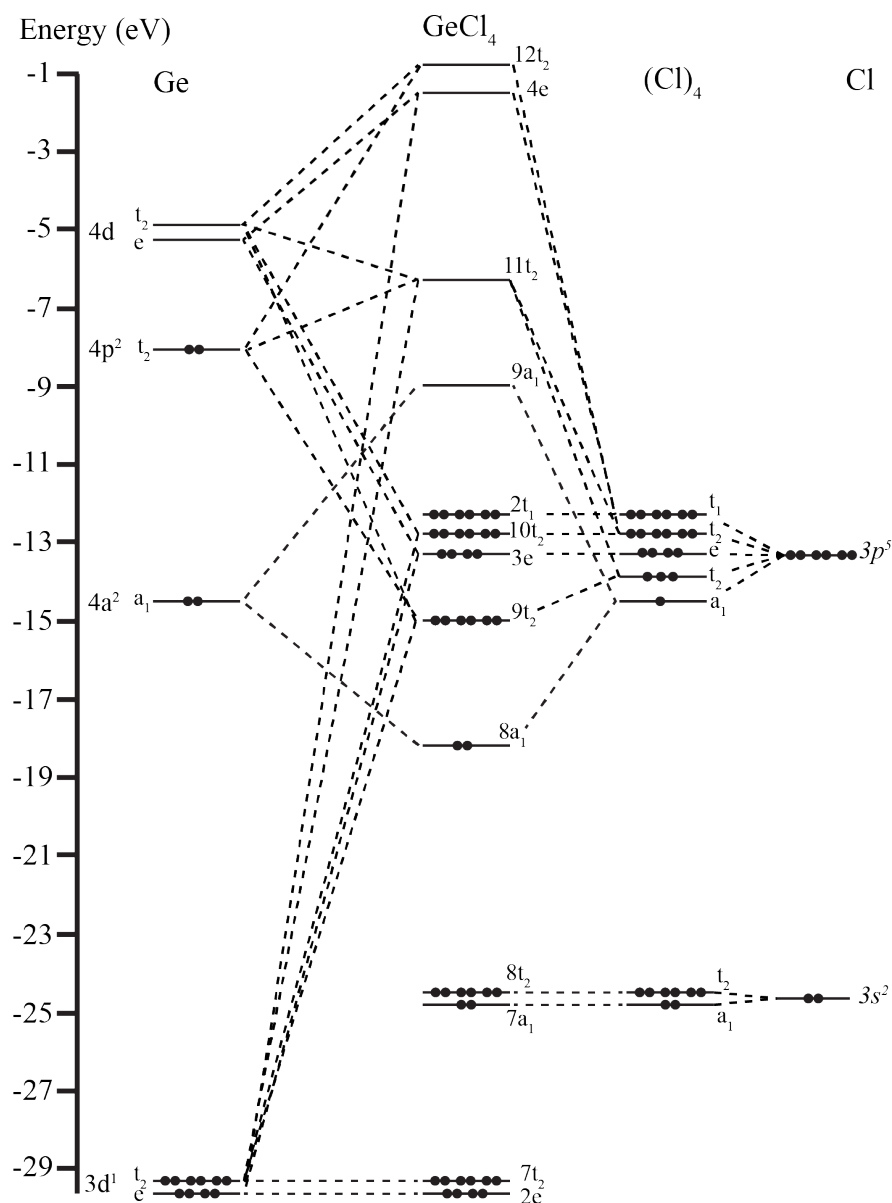


**Figure 1.1:** Qualitative molecular orbital diagram of GeCl<sub>4</sub> showing the electron configuration of the ground state of the molecule. Figure adapted from reference 10.

The structure of the current thesis study is such that a short theoretical overview of the formation of negative ions and their subsequent relaxation pathways is given, focusing on dissociative electron attachment. The experimental setup is then discussed along with calibration of the energy scale as well as fitting procedures for appearance energy determination. In addition to a positive ion mass scan and appearance energy fitting results, the last main chapter presents DEA ion yields from current measurements along with comparison to previous studies on the interaction of low-energy electrons with GeCl<sub>4</sub> and its congeners.

## 2 Theoretical Overview

### 2.1 Negative ion formation and decay

When an isolated gas phase molecule captures a low energy electron ( $\leq 15\text{eV}$ ), it forms a Transient Negative Ion (TNI). This interaction is a resonant process, which means that it can only take place in a specific energy range. The resulting anion is generally formed in an excited state and thus unstable in regards to relaxation. Relaxation pathways can generally be illustrated by the following reactions which show the formation of the transient negative ion and subsequent relaxation through Auto-Detachment (AD) or Dissociative Electron Attachment (DEA).



Electron attachment can be regarded as a vertical transition from the neutral ground state to the anionic state over a narrow energy range in the Franck-Condon (FC) region (see figure 2.1). The FC principle states that during a transition, the probability of an excitation from one state to another is proportional to the square of the overlap integral of the wave functions of the respective states. The energy difference between a neutral molecule (or atom) and its corresponding anion in their respective ground states is the Electron Affinity (EA) of the neutral molecule. In order for the anion to survive long enough for it to be detected by spectroscopic means, the anion must have positive EA, ensured by the anionic state being energetically lower than the neutral state. Resonances formed by the interaction of low energy electrons and molecules are classified into two categories based on the electron trapping mechanism: the mechanism by which the incident electron becomes temporarily trapped close to the molecule in a virtual, non-stationary state.

Figure 2.1 shows the formation and decay of the  $\text{MX}^{-*}$  resonance. As the transient negative ion travels along the purely repulsive potential shown in figure 2.1, there generally are two available relaxation channels: Auto-Detachment and the dissociation of the transient negative ion. Auto-Detachment, which is generally the most prominent relaxation channel, is the reemission of the electron as the molecule returns to its neutral state. If the transient negative

## 2 Theoretical Overview

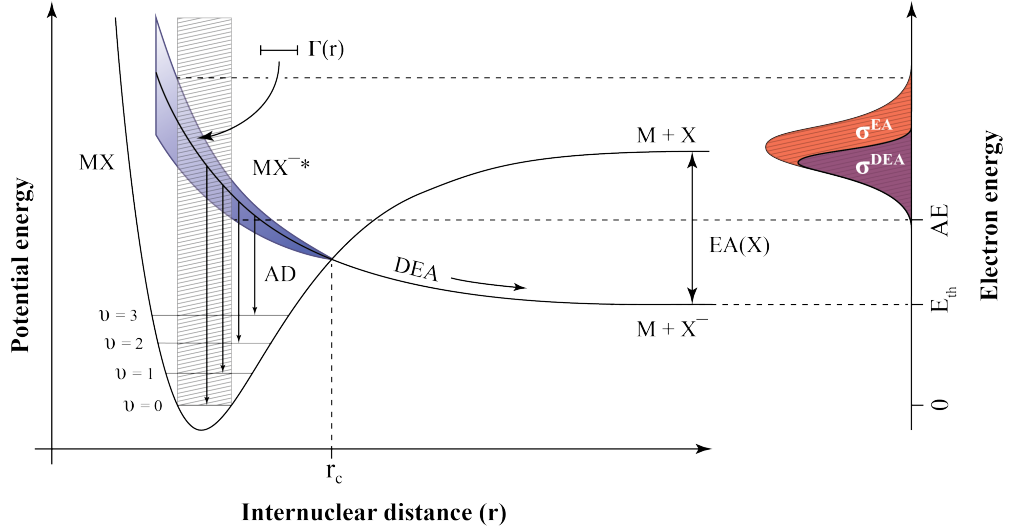


**Figure 2.1:** A schematic representation of the electron attachment to  $MX$  process and the subsequent relaxation, shown through Born-Oppenheimer potential energy diagrams. The possible relaxation pathways depicted are auto-detachment (AD) and dissociative electron attachment (DEA) where the TNI travels along the repulsive potential curve and past the crossing point ( $r_c$ ). The attachment and DEA cross sections are reflected by the Franck-Condon overlap of the respective potential curves shown on the right side of the figure and denoted with  $\sigma^{AE}$  and  $\sigma^{DEA}$ , respectively. The electron affinity of the charge carrying fragment is denoted with  $EA$ , the threshold energy with  $E_{th}$  and the appearance energy with  $AE$ . Figure adapted from reference 22.

ion relaxes to its ground state as the electron is reemitted with the same energy it had before interacting with the molecule, the electron is elastically scattered. Otherwise, if the neutral molecule retains some of the energy by becoming vibrationally, rotationally or electronically excited, then the electron is inelastically scattered. The lifetime of the resonance with respect to auto-detachment,  $\tau_{AD}$ , given by the Heisenberg principle, is inversely related to the width of the resonance ( $\Gamma$ ):

$$\tau_{AD} \propto \frac{\hbar}{\Gamma}. \quad (2.3)$$

If the transient negative ion survives long enough to travel along the repulsive potential and pass the crossing point of the anionic and the neutral curve ( $r_c$ ), it is bound to dissociate through the rupture of one or more chemical bonds, i.e, dissociative electron attachment (DEA). This results in the formation of a negatively charged fragment ( $X^-$ ) and a neutral counterpart ( $M$ ). The chance of DEA happening, i.e the resonance's survival probability ( $P$ ), depends on the lifetime with respect to auto-detachment ( $\tau_{AD}$ ) and the time it takes to reach the crossing point ( $t$ ):

$$P = e^{-\tau_{AD}/t}. \quad (2.4)$$

## 2 Theoretical Overview

In other words, DEA measures the yield of long-living anionic fragments produced by dissociation of the resonance as a function of electron impact energy.

The minimum energy required for dissociation of a chemical bond is the dissociation threshold ( $E_{th}$ ) and by use of the thermochemistry of the DEA process, for a diatomic molecule it can be expressed as the bond dissociation energy (BDE) less the electron affinity of the charge carrying fragment (EA). In a polyatomic molecule on the other hand, multiple bonds may be ruptured and others formed, and thus the expression for the threshold energy takes the form:

$$E_{th} = \sum^N \text{BDE}(\text{educt}) - \sum^M \text{BDE}(\text{product}) - \text{EA}(\text{X}) \quad (2.5)$$

However, dissociation channels commonly appear at higher energies than the dissociation threshold would suggest. This is due to the fact that the attachment is a resonant process that may be confined to an electron energy range well above the dissociation threshold, causing the relaxation channel to be closed until sufficient energy is available for dissociation of the resonance. Nevertheless, if the threshold falls within the energy range of the resonance in question, the appearance energy will be defined by the threshold energy rather than the transition probability within the Franck-Condon region. The lowest energy that a given anion is observed at in the ion yield is the appearance energy (AE) and can also be described as the sum of the threshold energy and some additional energy. This additional energy will be on the form of the kinetic energy of the fragments ( $E_{kin}$ ) and their internal energy ( $E_{int}$ ). To account for this, equation 2.5 can be expanded to take the form:

$$\text{AE} = \sum^N \text{BDE}(\text{educt}) - \sum^M \text{BDE}(\text{product}) - \text{EA}(\text{X}) + E_{kin} + E_{int}. \quad (2.6)$$

## 2.2 Negative ion resonances

In electron attachment, the transient negative ion ( $\text{MX}^{-*}$ ) can generally be characterized by its electron configuration (see figure 2.2). If the incident electron occupies a previously unoccupied molecular orbital it is a one particle resonance. However, if another electron is excited from one of the previously occupied orbitals in the process, leaving a hole in its stead, it is referred to as a two particle one hole resonance, also known as a core-excited resonance. Resonances can then be further categorized as shape or Feshbach resonances, depending on the electron trapping mechanism. When discussing resonant states, the concept of *parentage* often comes up. For a given transient negative ion state, there exist a neutral state (ground or excited) whose electron configuration differs only with respect to the attached electron. Here, the neutral state ( $\text{MX}$ ) is the parent state of the resonance ( $\text{MX}^{-}$ ).

## 2 Theoretical Overview

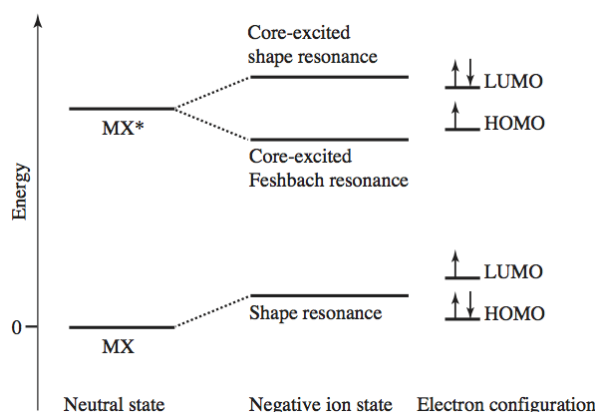


**Figure 2.2:** Schematic figure of resonant states on an arbitrary energy scale showing their electron configuration and relative energetical position. Figure taken from reference 23 © Frímann Haukur Ómarsson .

A shape resonance forms when the incident electron is trapped within a centrifugal potential barrier. The free electron can be seen as a wave packet composed of a linear combination of partial waves, i.e. waves with different values of the angular momentum quantum number ( $l = 0, 1, 2, 3, \dots$ ). If a molecule possesses an energetically accessible unoccupied molecular orbital, characterized through its symmetry by a given combination of angular momentum values ( $l$ ), then an incoming electron of the same  $l$  value combination can be temporarily captured within the barrier. In simple terms, the electron - molecule interaction can be described by two potentials: an attractive polarization potential and the repulsive centrifugal potential associated with the angular momentum of the orbital:

$$V(r) = -\frac{\alpha}{2r^4} + \frac{l(l+1)}{2r^2}. \quad (2.7)$$

Here,  $\alpha$  is the polarizability of the atom/molecule and  $r$  is the electron-molecule distance.<sup>24</sup> To become trapped, the electron has to tunnel through the angular momentum barrier; in the absence of such a barrier ( $l = 0$ ), no electron trapping takes place (see figure 2.3). As the electron passes this barrier and gets closer to the molecule, there is also a repulsive potential due to the Pauli exclusion principle creating a strong repulsive force at short nuclear distances. As the electron is trapped between the repulsive Coulomb potential and the centrifugal barrier, the lifetime of a transient negative anion is highly dependent on both its internal energy and the size of the potential barrier. Because these resonances are energetically above their corresponding neutral state, they decay efficiently through auto detachment (AD, see section 2.1) which results in a short lifetime of the resonance. Shape resonances occur normally between 0-4 eV, with only a few notable exceptions.<sup>25</sup> A shape resonance can be associated with concomitant excitation of a core electron as the incoming electron is

## 2 Theoretical Overview

captured (i.e. core-excitation) or the direct capture of a single electron.

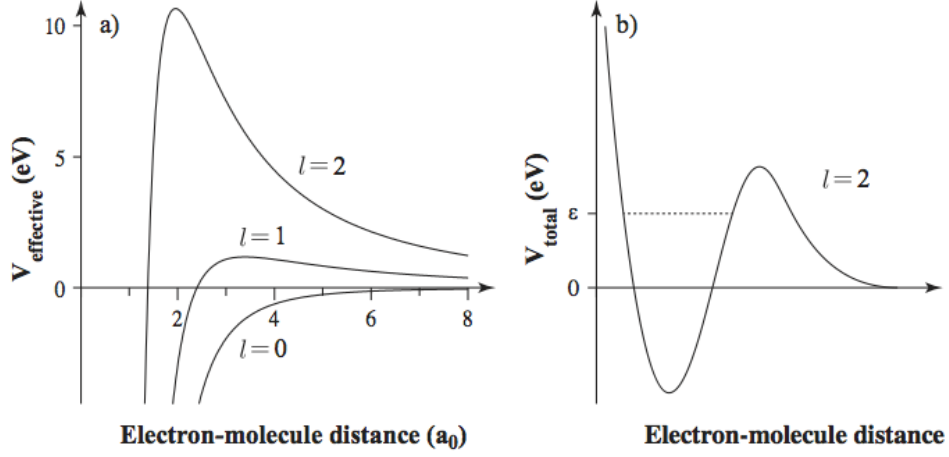


**Figure 2.3:** Left: A graph showing the angular momentum dependency of the centrifugal potential barrier ( $V_{\text{effective}}$ ). Right: an example of the total interaction potential ( $V_{\text{total}}$ ) for d-wave attachment ( $l = 2$ ) with a certain energy  $\epsilon$ . Figure taken from reference 22. © Benedikt Ómarsson.

In contrast to shape resonances, if a core-excited resonance is formed energetically *below* the neutral parent state, decay of this resonance must proceed through a change in electronic configuration. This requires additional energy, and thus, auto-detachment is not possible. Such a resonance is referred to as a closed-channel resonance or a Feshbach resonance.

## 3 Methods

### 3.1 Experimental setup

All measurements presented in this thesis were conducted on a high-vacuum crossed-beam electron apparatus termed SIGMA (Simply A Gas phase MACHine), constructed by Elías H. Bjarnason as a part of his PhD work and thoroughly described in reference.<sup>26</sup> The device consists of a Trochoidal Electron Monochromator<sup>27</sup> (TEM), a collision region and a HIDEN Epic 1000 quadrupole mass spectrometer equipped with a channeltron detector. Although the TEM is monochromator by name, it functions more as a velocity selector. A schematic of SIGMA can be seen in figure 3.1. The background pressure of the chamber is on the order of  $10^{-8}$  mbar, while experiments are performed at a pressure on the order of  $10^{-7}$  mbar. To ensure single collision conditions, the pressure is kept below  $10^{-7}$  mbar, putting the mean free path of the target molecule on the order of 1 km, which exceeds the dimensions of the measuring apparatus. Electrons with an energy distribution of 0.5 to 1 eV are emitted from a hairpin tungsten filament, slightly focused by M2 and M3 and collimated by a constant magnetic field  $\mathbf{B}$  of  $\sim 50$  Gauss generated by two magnetic coils. The electron beam then enters an electric field  $\mathbf{E}$  between lenses M5 and M6 that is orthogonal to  $\mathbf{B}$ . This causes them to drift on a trochoidal trajectory with constant velocity in a direction orthogonal to both the electric and magnetic fields. The energy distribution of the electron beam causes some electrons to travel faster than others through  $\mathbf{B} \times \mathbf{E}$  field. These electrons exit this region earlier and have thus had less time to drift off their axis. This results in a fan of electrons as can be seen in figure 3.1. A narrow slice of the energy distribution is selected by the exit slit of M7 being offset from the entrance of M4 by 2.4 mm. The actual resolution of the electron beam is adjusted by careful tuning of the voltage on crucial monochromator lenses. After passing through the monochromator lenses, the electrons energy is controlled by a voltage difference between the M and C lenses. During a negative ion scan, the voltage between the lenses is ramped from 0 to 10 volts, which defines the kinetic energy of the electrons in the collision region. The electrons then interact with an effusive gas beam and the anions formed are extracted by a weak electric field between C2 and C3 and focused with circular electrodes (F1-F3) to a quadrupole mass spectrometer. In the quadrupole, the anions are separated based on the stability of their trajectories in the oscillating electric fields that are induced by an RF voltage applied between opposite pairs of rods. Only a specific mass per

### 3 Methods

charge ratio will reach the channeltron detector (electron multiplier) where one anion sparks a flurry of electrons, creating a signal that is sent to a computer and observed on screen.

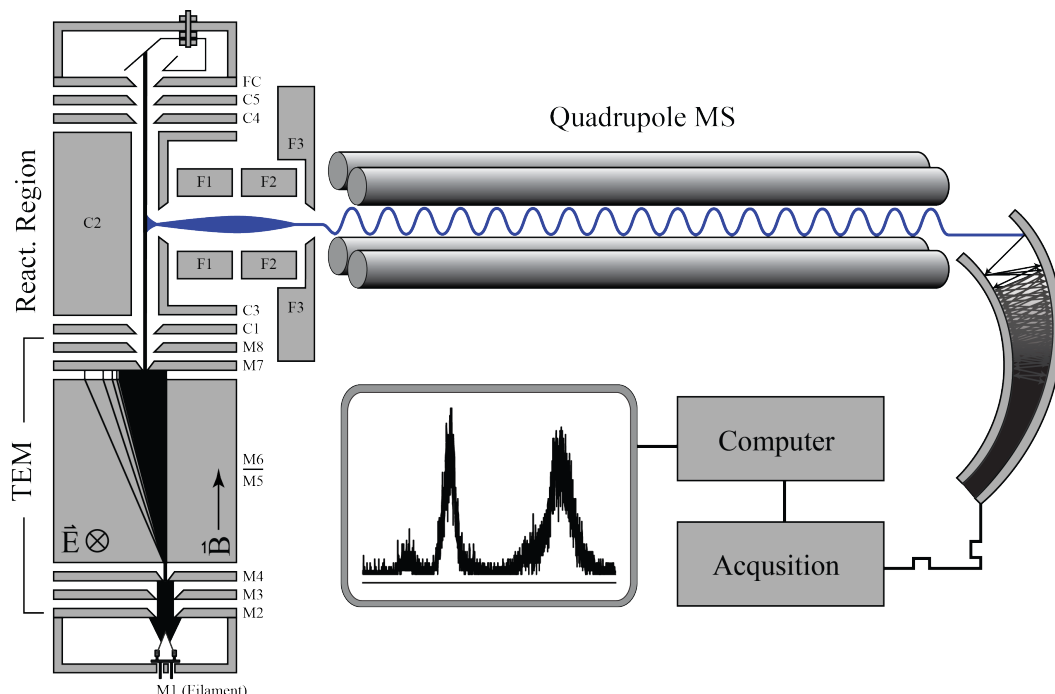


**Figure 3.1:** A schematic of the apparatus (SIGMA) used to measure the negative ion formation from DEA to  $\text{GeCl}_4$  in this thesis study. Figure taken from reference 22. © Benedikt Ómarsson

The  $\text{GeCl}_4$  used in this experiment was purchased from Sigma Aldrich with a stated purity of 99.99%.  $\text{GeCl}_4$  is a clear liquid at STP conditions but is very hygroscopic; therefore, the sample had to be loaded into the sample holder inside a glovebox filled with inert argon. During measurements, the sample was dosed into the collision region through a precision leak valve to maintain a stable pressure.

## 3.2 Energy Calibration

The electron energy scale was calibrated using a three point calibration method. The first fixed point is the contribution of a 0 eV resonance in the ion yield of  $\text{SF}_6^-$  from  $\text{SF}_6$ .<sup>28</sup> The zero point of the electron energy scale was set by fixing the peak of the  $\text{SF}_6^-$  contribution to 0 eV prior to measurements. This was done by adjusting the floating reference voltage ( $V_R$ ), to which the monochromator lenses (M2-M8) are referenced. Two resonances leading to the formation of  $\text{O}^-$  from  $\text{CO}_2$  at 4.4 and 8.2 eV, respectively<sup>29</sup> provided the other two fixed calibration points. The measured peak values of the two contributions were used as fixed points to calibrate the upper part of the energy scale. The shape of the contribution at 4.4 eV

### 3 Methods

is quite complex, but a more detailed spectra provided by Cicman *et al.*<sup>30</sup> was used to help accurately determine the correct peak value. To account for possible shift of the energy scale during a measurement due to charging effects on the monochromator lenses, both the  $\text{SF}_6^-$  and  $\text{O}^-$  yields were measured before and after each DEA measurement and the average of the peak values were used to calibrate the energy scale. This calibration had the largest effect on the energy scale around 4.4 eV because the contribution from the resonance consistently appeared at a value 0.1-0.2 eV below its nominal value while the peak of the contribution at 8.2 eV was mostly recorded at its predicted value. An example of the calibration ion yields can be seen below in figure 3.2.

In a DEA measurement, the measured signal is a convolution of the electron beams energy distribution and the shape of the resonances contribution to the ion yield. It was determined by Klar *et al.*<sup>28</sup> that the width of the  $\text{SF}_6^-$  resonance is  $< 1$  meV, so the width of the  $\text{SF}_6^-$  signal measured is an excellent approximation of the width of the electron beams energy distribution. The Full Width at Half Maximum (FWHM) of  $\text{SF}_6^-$  is used to determine the resolution of the energy signal. In the first measurements a typical FWHM of the  $\text{SF}_6^-$  signal acquired was 130 meV, but over the course of the measurements the resolution was gradually improved and reached 80 meV in the last measurements.

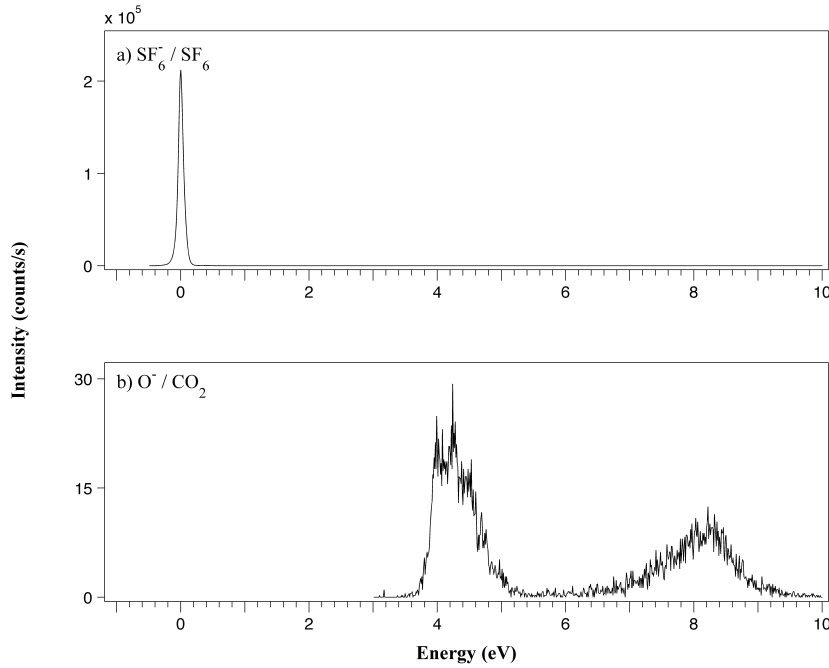


**Figure 3.2:** An example of the ion yields of  $\text{SF}_6^-$  from  $\text{SF}_6$  and  $\text{O}^-$  from  $\text{CO}_2$  in the relevant energy range that were used to calibrate the electron energy scale

### 3.3 Determination of Appearance Energy

One of the main goals of the current thesis study was to determine the appearance energy (AE) of all resonances as they appear in the ion yield of every fragment formed through DEA to  $\text{GeCl}_4$ . In a DEA measurement, the appearance energy is the lowest electron energy that a given anion is observed at. In the current thesis work, two fitting methods were used to reproduce the onset region of the ion yield curves, an exponential function and a linear fitting function. Every fragments ion yield was measured on three different occasions and fitted separately with both functions. The end result was an average of the determined appearance energy values obtained and is presented separately for each function. The error estimation was based on the difference between the fits. The first approach used to determine the appearance energy is a Wannier-type function, which is basically an exponential function with a scaling factor. The Wannier function was originally derived as a threshold law for photo-ionization processes.<sup>31</sup> Nonetheless, we find it to reproduce the onset of the ion yield curve fairly well. A drawback of the Wannier function is that it needs a stable baseline before the onset of the resonance, which is not always present. The function takes the form:

$$f(E) = b + a(E - AE)^d, \quad (3.1)$$

where  $b$  is a constant that takes into account the background signal,  $a$  is a scaling coefficient,  $E$  is the energy of the incident electron and  $d$  is an exponential factor. To account for the finite energy resolution of the electron beam, equation 3.1 was convoluted with a Gaussian of the same FWHM as the  $\text{SF}_6^-$  resonance recorded for each measurement. A fitting script written by E. H. Bjarnason was used to convolute the equation and fit the onset of the resonances. The second approach was based on a linear fit, which uses a simple linear regression model where two points in the ion yield are selected at the onset of the resonance; one at the very first indication of a signal and the other slightly further along the onset, but before the ion yield curve starts to rise with a constant slope. Using a conventional least-square method, the intensity values between the two points are regressed onto the energy values. The fitted line (see equation 3.2) was then extrapolated to find the intersect with the baseline of the signal, which is taken as the appearance energy of the ion yield curve. Since choosing where to select the two points on the ion yield curve had to be gauged visually, three individual linear fits were made to every dataset and an average of the three used as the final result. Here the linear fitting equation is shown, where  $k$  is the slope of the line and  $m$  is the intersect with the y-axis:

$$f(E) = kE + m. \quad (3.2)$$

## 4 Results And Discussion

In the previous chapters, the theory behind negative ion formation and dissociative electron attachment has been presented as well as a description of the experimental setup and the fitting procedures. This chapter will present results from current measurements and compare them with earlier studies. The first section deals with the positive ion mass spectrum of  $\text{GeCl}_4$  recorded to determine its purity and composition. In the second section, the application of the fitting procedure and its limitations will be discussed. The third section constitutes the bulk of the thesis work and presents ion yields obtained from the DEA measurements of  $\text{GeCl}_4$  along with discussions of observed features in context with earlier studies where available.

## 4.1 Positive ion mass scan

Before taking negative ion spectra a positive ion electron ionization mass spectrum of  $\text{GeCl}_4$  was recorded with SIGMA in order to examine Dissociative Ionization (DI) of the target molecule and establish its purity (see figure 4.1). To achieve this, an electron beam with a fixed energy of  $\sim 70$  eV was used to bombard the molecules causing them ionize and subsequently dissociate due to the extra energy in excess of the ionization energy. The spectrum was recorded at a sample pressure of  $5 \times 10^{-7}$  mbar.

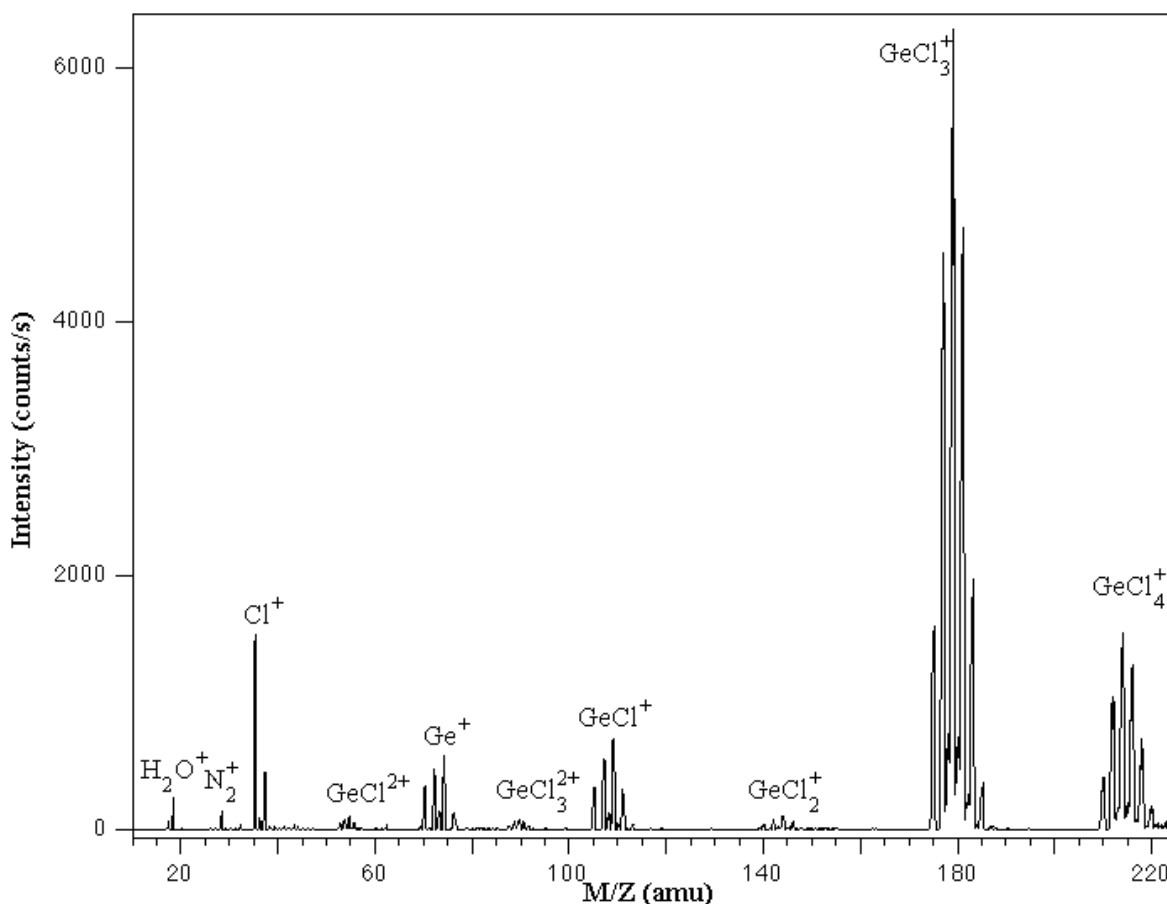


**Figure 4.1:** Dissociative Ionization spectrum of  $\text{GeCl}_4$  recorded at 70 eV impact energy.

In the DI spectrum of  $\text{GeCl}_4$  shown in figure 4.1, every possible positive fragment resulting from dissociative ionization of  $\text{GeCl}_4$  is observed:  $\text{GeCl}_{4-n}^+$ ,  $n = 0, 1, 2, 3, 4$ . Also present are the  $\text{Cl}^+$  ion and the doubly-charged  $\text{GeCl}^{2+}$  and  $\text{GeCl}_3^{2+}$  ions. Comparison of the current mass spectrum with an electron ionization mass spectrum available in the literature<sup>32</sup> shows that all possible fragments are observed with good resolution and that the collision chamber is clear of other contaminants, besides a small signal of residual air ( $\text{N}_2^+$  and  $\text{H}_2\text{O}^+$  peaks).

## 4.2 Determination of the appearance energy

The appearance energy was determined by fitting the onset of the ion yield curves of every fragment. Each fragments ion yield was measured on three separate occasions and thereafter fitted individually. Every ion yield was fitted independently with a Wannier-type function and a linear fitting function. The error margins were estimated by the mean deviation of the recorded appearance energies and the ‘goodness of the fits’. The error margins are estimated to be 0.1 eV for the appearance energy of every fragment except  $\text{Cl}_2^-$ , where it was estimated to be 0.2 eV due to the low intensity of the ion yield curve. It should also be noted that the 1.4 eV contribution in the  $\text{GeCl}_3^-$  yield could not be fitted with the Wannier-type function because of an overlap with a 0 eV contribution and was therefore only fitted linearly. Figure 4.2 shows an example of good results from both fitting methods for the onset of a contribution observed in the ion yield of  $\text{GeCl}_3^-$ . The determined appearance energies of all contributions are presented in table 4.1 in chapter 4.3. By using two independent approaches that expectantly return the same value for the appearance energy, we believe that additional certainty is given to our values.

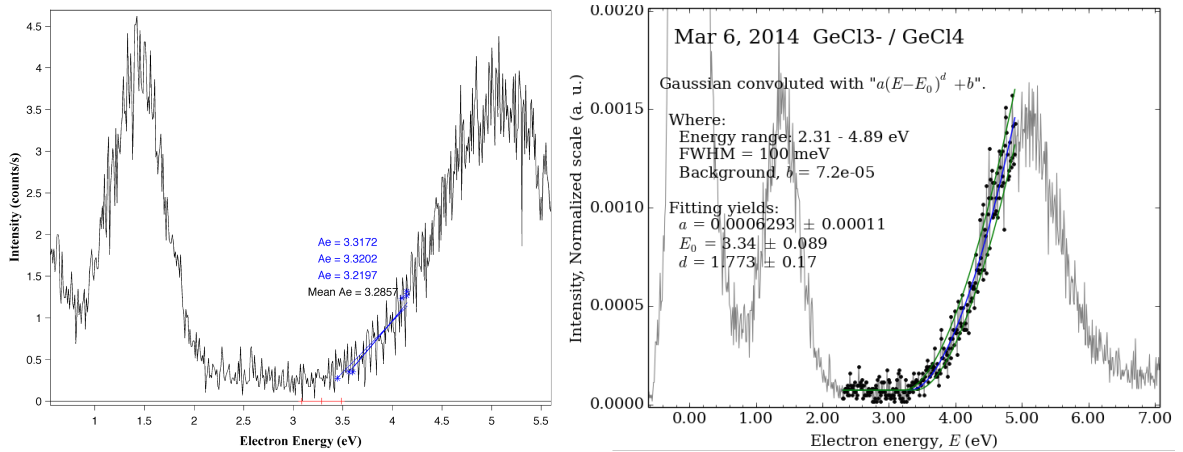


**Figure 4.2:** Appearance energy determined by fitting the onset of an ion yield curve in the  $\text{GeCl}_3^-$  yield. Left figure shows the results from a linear fitting function and a Wannier-type fitting function is shown on the right. The figures are direct printouts from fitting programs and the significant numbers shown are in some cases not reasonable.

While the Wannier-type and the linear fitting functions reproduce the onset of most ion yield curves adequately, both functions have some limitations. In the case of  $\text{Cl}^-$ , the onset was not well reproduced by the Wannier-type function. The contribution rises slowly at  $\sim 3.4$  eV and then sharply increases at  $\sim 3.6$  eV. The Wannier-type function overestimates the appearance energy as can be seen in figure 4.3 where the fitting function diverges from the onset near what seems to be the actual appearance energy.

## 4 Results And Discussion

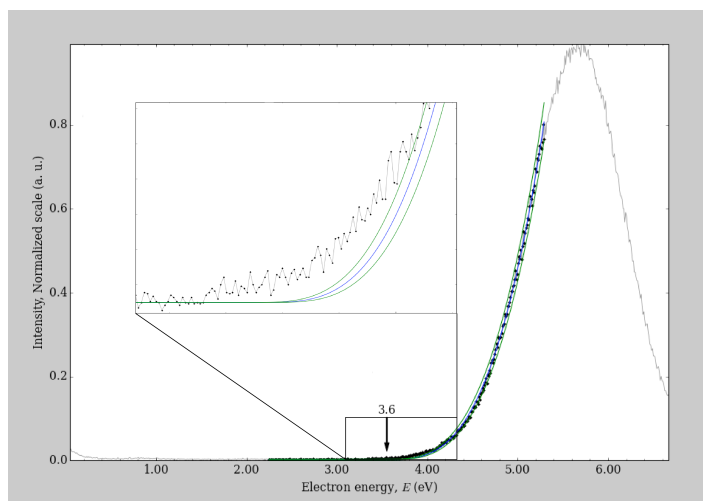


**Figure 4.3:** The limitations of fitting the onset of the  $\text{Cl}^-$  contribution with a Wannier-type function. The Wannier-type function diverges from the ion yield curve near the actual onset of the contribution.

A different problem was observed for the 1.4 eV contribution in the  $\text{GeCl}_3^-$  yield due to overlap with the 0 eV contribution (see figure 4.4). The onset of the higher lying ion yield curve is lost in the tail of the 0 eV peak and therefore the linear fitting function had to be applied to a upper part of the ion yield curve. This most likely results in an overestimation of the appearance energy, and thus, causes an increase in the estimated error margin.

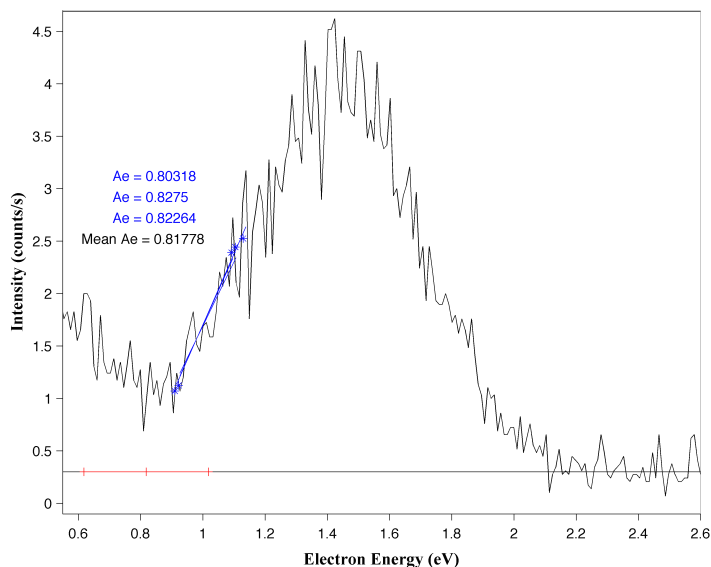


**Figure 4.4:** Linear fit of a contribution to the  $\text{GeCl}_3^-$  yield. Due to overlap with a 0 eV contribution, a higher part of the contribution was fitted causing an overestimation of the appearance energy.

### 4.3 Dissociative electron attachment to $\text{GeCl}_4$

In the current measurements of dissociative electron attachment to  $\text{GeCl}_4$ , three resonances were detected. These were observed through contributions centered at  $\sim 0$  eV, 1.4 eV and  $\sim 5$ -6 eV. Figure 4.5 shows the ion yields of the four observed fragments,  $\text{GeCl}_3^-$ ,  $\text{Cl}^-$ ,  $\text{GeCl}_2^-$  and  $\text{Cl}_2^-$  in order of their respective intensity. The appearance energies of each contribution are presented in table 4.1. Each fragment's ion yield was measured on three different occasions with the number of scans ranging from 15 to 40, depending on the intensity of the signal. The signal intensity is linearly dependent on the pressure in the collision region, and while the samples were measured with varying sample pressure (from  $5 \times 10^{-7}$  mbar to  $1.2 \times 10^{-6}$  mbar), their signal intensity was normalized to a nominal pressure of  $7 \times 10^{-7}$  mbar. However, care should be taken when comparing the relative intensities of 0 eV contributions and signals of higher energy since the 0 eV signal is strongly dependent on the onset of the electron beam. In this section, the current results will be put into context by a brief overview of the results from earlier studies related to low-energy electron interaction with  $\text{GeCl}_4$ . Thereafter, the results from the current measurements will be discussed by addressing individually the three energy ranges where the resonances appear.

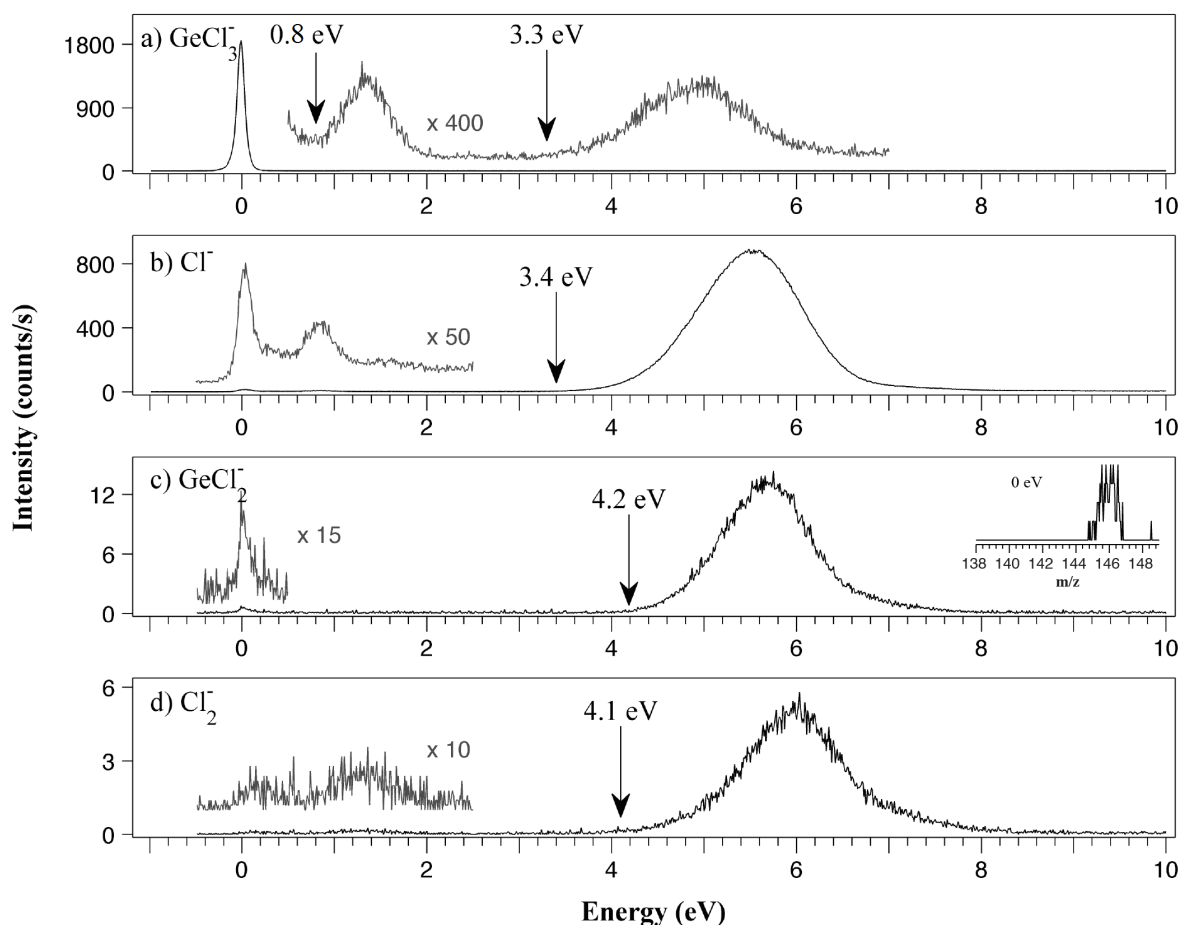
**Table 4.1:** Appearance energies (AE) determined from the onset of ion yield curves by use of (a) Wannier-type and (b) linear fitting functions. \*Note that the Wannier-type function overestimates appearance energy of  $\text{Cl}^-$  by  $\sim 0.2$  eV

<b>(a) Wannier-type fit</b>					
Meas.	i) $\text{GeCl}_3^-$	ii) $\text{GeCl}_3^-$	$\text{Cl}^-$	$\text{GeCl}_2^-$	$\text{Cl}_2^-$
1	-	3.32	3.65	4.18	4.17
2	-	3.34	3.63	4.25	4.02
3	-	3.26	3.55	4.23	-
<b>Mean AE</b>		$3.3 \pm 0.1$	$3.6 \pm 0.1^*$	$4.2 \pm 0.1$	$4.1 \pm 0.2$

<b>(b) Linear fit</b>					
Meas.	i) $\text{GeCl}_3^-$	ii) $\text{GeCl}_3^-$	$\text{Cl}^-$	$\text{GeCl}_2^-$	$\text{Cl}_2^-$
1	0.77	3.29	3.49	4.15	4.14
2	0.80	3.30	3.31	4.27	4.08
3	0.82	3.29	3.34	4.22	-
<b>Mean AE</b>	$0.8 \pm 0.2$	$3.3 \pm 0.1$	$3.4 \pm 0.1$	$4.2 \pm 0.1$	$4.1 \pm 0.2$

## 4 Results And Discussion



**Figure 4.5:** Dissociative electron attachment ion yield curves for  $\text{GeCl}_4$  in the energy range of  $\sim 0$  to 10 eV. The grey lines show a scaled part of the ion yield for better visual analysis and the arrows indicate the estimated appearance energies. The features observed in these ion yields are discussed in the text.

As was mentioned in the introduction, two dissociative electron attachment studies on  $\text{GeCl}_4$  have previously been conducted. In the first, Pabst *et al.*<sup>9</sup> examined the ion yields of four fragments ( $\text{GeCl}_3^-$ ,  $\text{Cl}^-$ ,  $\text{GeCl}_2^-$  and  $\text{Cl}_2^-$ ) in the range of 1 - 10 eV. They observed a contribution in the ion yields of all four fragments around 5-6 eV as well as a lower energy contribution in the ion yield of  $\text{GeCl}_3^-$  at  $\sim 2$  eV. In the second study, Guillot *et al.*<sup>10</sup> recorded the ion yields of three fragments ( $\text{GeCl}_3^-$ ,  $\text{Cl}^-$  and  $\text{GeCl}_2^-$ ) in the energy range of  $\sim 0$  - 10 eV, and to a certain extent, observed dissimilar results to those obtained by Pabst *et al.*<sup>9</sup>. Guillot *et al.* recorded a contribution at  $\sim 0$  eV in the  $\text{GeCl}_3^-$  yield and around 5-6 eV in both the  $\text{Cl}^-$  and  $\text{GeCl}_2^-$  ion yields. The higher lying resonances of  $\text{GeCl}_3^-$  and  $\text{Cl}_2^-$  were not observed, most likely due to lack of sensitivity. Pabst *et al.*<sup>9</sup> on the other hand, failed to detect the 0 eV resonance because they were limited to electron energies above 1 eV. Complementary to their DEA studies, Guillot *et al.*<sup>10</sup> identified the symmetries of the highest

## 4 Results And Discussion

occupied and lowest unoccupied molecular orbitals of  $\text{GeCl}_4$  using X-ray absorption spectra (XAS). Additionally, they observed two resonances centered around 1.7 and 5.6 eV, respectively, using electron transmission spectroscopy (ETS). Those results corresponds well with a total electron scattering cross section study by Szmytkowski *et al.*<sup>12</sup> which shows a distinct resonance maxima at 1.7 eV and another broader peak at 9 eV with a noticeable shoulder at 6 eV. Joining their results from DEA, ETS and XAS, Guillot *et al.* assigned symmetries to the three observed resonances of  $\text{GeCl}_4$ . The 0 eV resonance was attributed to the single electrons occupation of the  $a_1$  LUMO and similarly, the resonance at 1.7 eV was accredited to the extra electron occupying the  $t_2$  LUMO+1 orbital. The nature of the higher energy resonance at 5-6 eV could not be precisely determined. Guillot *et al.* offered two possible explanations.

The first possibility is that the resonance is core-excited because of its relatively high energy. The other possibility is a high energy shape resonance, where the electron temporarily occupies a 4e orbital, which has strong Ge d character. The high potential barrier associated with this shape resonance can account for its high energy. The second assumption is supported by the absence of this resonance in  $\text{CCl}_4$ ,<sup>33</sup> due to the lack of low-energy d orbitals in the carbon atom. However, independent of the trapping mechanism, the resonance is thought to be of E symmetry.

### 4.3.1 Ion yield at around 0 eV

From the intensity of the 0 eV contribution in the  $\text{GeCl}_3^-$  yield in the current measurement, it is evident that the cross section of  $\text{GeCl}_4$  at 0 eV is very high and the dominant dissociative relaxation channel results in the formation of  $\text{GeCl}_3^-$ . The dissociation energy of the  $\text{GeCl}_3-\text{Cl}$  bond has been estimated to be  $3.64 \pm 0.52$  eV,<sup>34</sup> and thus, to rupture the bond, the electron affinity of the anion must be greater than  $3.64 \pm 0.52$ . The only experimental value to date for the electron affinity of  $\text{GeCl}_3^-$  was estimated by Pabst *et al.*<sup>9</sup> to be 1.8 eV. However, because they did not observe the 0 eV resonance, they estimate the threshold from a higher lying resonance and thus, clearly underestimate the electron affinity of  $\text{GeCl}_3$ . A calculated value provided by NIST<sup>35</sup> offers a more probable value of  $\sim 3.7$  eV and this is supported by our own B3LYP calculations which returned an electron affinity of 3.76 eV. Since the electron affinity of  $\text{GeCl}_3$  is greater than the bond dissociation energy, the dissociation channel is open, giving rise to an intense signal in the  $\text{GeCl}_3^-$  yield.

This resonance is also observed in the ion yield of  $\text{Cl}^-$ , although with considerably lower intensity. In the current instrumental setup the ion extraction efficiency is highly dependent on the kinetic energy of the fragments (i.e. Kinetic energy release), and as the mass ratio of  $\text{Cl}^-$  to  $\text{GeCl}_3^-$  is roughly 1:5, the  $\text{Cl}^-$  fragments carries the bulk of kinetic energy. However, we point out that the formation of these ions at  $\sim 0$  eV is not likely to be associated with

#### 4 Results And Discussion

considerable excess energy. The electron affinity of Cl is the highest of all elements and has been well established as 3.613 eV.<sup>36</sup> However, it does not provide enough energy to rupture a  $\text{GeCl}_3\text{--Cl}$  bond and so the dissociation channel is supposedly closed. This resonance has not been detected in the ion yield of  $\text{Cl}^-$  before and Guillot *et al.*<sup>10</sup> stated that even though the formation of a neutral  $\text{GeCl}_3$  fragment and a charged  $\text{Cl}^-$  might be energetically allowed at 0 eV, it is most likely kinetically prohibited. We however, find it more likely that the difference in the intensity of the  $\text{GeCl}_3^-$  and  $\text{Cl}^-$  peaks is rooted in the thermochemical threshold of these processes. We propose that the BDE of the  $\text{GeCl}_3\text{--Cl}$  bond is at the higher limit of the error margin reported and that the EA of  $\text{GeCl}_3$  is sufficiently high to account for bond rupture. The EA of Cl on the other hand, is not able to account for bond rupture but considering the high error margin of the BDE, we conclude that the signal in the  $\text{Cl}^-$  yield is most likely due to Hot Band transitions, i.e., some molecules in the collision chamber being ‘hotter’ than others (assuming Boltzmann distribution), providing the extra energy needed to rupture the bond.

Contrary to what was determined for  $\text{GeCl}_3^-$  and  $\text{Cl}^-$ , the 0 eV contribution in the  $\text{GeCl}_2^-$  yield can not be accounted for by the resonances of  $\text{GeCl}_4$  since the electron affinity of  $\text{GeCl}_2$  found by calculations and provided by NIST has been estimated to be 1.3 eV,<sup>37</sup> and thus, the resonance can not dissociate at this energy. To verify if the isotope distribution of this signal matches that for  $\text{GeCl}_2$ , a mass scan with fixed 0 eV electron energy was conducted and can be seen in an inset in the ion yield of  $\text{GeCl}_2^-$  in figure 4.5. The mass scan shows that no  $\text{GeCl}_2^-$  was present at 0 eV. We thus conclude that the signal is from residual  $\text{SF}_6$  used for calibration prior to the measurement. The sulfur in  $\text{SF}_6$  has an  $^{34}\text{S}$  isotope that constitutes 4.21% of the sulfur content.  $^{34}\text{SF}_6^-$  has the same mass per charge ratio as  $\text{GeCl}_2^-$  and due to its high cross section, appeared in the  $\text{GeCl}_2^-$  ion yield.

A very weak signal was also detected in the ion yield of  $\text{Cl}_2^-$  around 0 eV with a slight but noticeable shift towards higher energy. Equation 2.5 from chapter 2.1 can be used to determine the thermochemical threshold for the formation of a  $\text{Cl}_2^-$  ion. The dissociation energies of the  $\text{GeCl}_3\text{--Cl}$  and  $\text{GeCl}_2\text{--Cl}$  bonds have been estimated by Gurvich *et al.*<sup>34</sup> to be  $3.64 \pm 0.52$  and  $2.25 \pm 0.52$  eV, respectively. The bond dissociation energy of the formed  $\text{Cl}_2$  is  $2.51 \pm 0.08$  eV<sup>38</sup> and the electron affinity of  $\text{Cl}_2$  has been estimated to be  $2.5 \pm 0.2$  eV.<sup>39</sup> Hence, the threshold energy for the formation of  $\text{Cl}_2^-$  is calculated to be 0.88 eV. The low intensity and the energy shift of the observed peak can therefore be accounted for by Hot Band transitions.

The nature of the 0 eV resonance appearing through the ion yields from  $\text{GeCl}_4$  is comparable with the DEA to  $\text{GeBr}_4$  spectra recorded by Ómarsson *et al.*<sup>2</sup> There, a similar situation was observed where a low-energy contribution in the  $\text{GeBr}_3^-$ ,  $\text{Br}^-$  and  $\text{Br}_2^-$  yields was recorded peaking at  $\sim 0.5$  eV. The dissociation energy of the  $\text{GeBr}_3\text{--Br}$  bond was calculated to be 3.30 eV while the electron affinities of Br and  $\text{GeBr}_3$  were calculated as 3.44 eV and 3.74 eV,

## 4 Results And Discussion

respectively. Thus, in agreement with calculated threshold, the energetically most favorable channel dominates.

### 4.3.2 Ion yield at around 1.4 eV

A resonance located at 1.4 eV appears in the ion yield of  $\text{GeCl}_3^-$  as a low-intensity peak. This contribution most likely stems from the same  $T_2$  resonance as was observed with electron transmission and in the total cross section spectra discussed in the text above. The same resonance is observed in the current  $\text{Cl}_2^-$  ion yield with very low intensity but no signal is detected in the  $\text{GeCl}_2^-$  yield.

The possible formation of  $\text{Cl}^-$  through a contribution to the ion yield at 1.4 eV can not be distinguished due to interference with a signal at  $\sim 1$  eV which we assign to residual HCl formed through hydrolysis of  $\text{GeCl}_4$  in the inlet system. When working with  $\text{GeCl}_4$ , there is always a chance of HCl forming in the inlet system as  $\text{GeCl}_4$  reacts with residual water vapor. The DEA spectrum of HCl<sup>40</sup> has previously been recorded with high precision (see figure 4.6) and shows a contribution that very accurately resembles the signal seen in the current measurement.

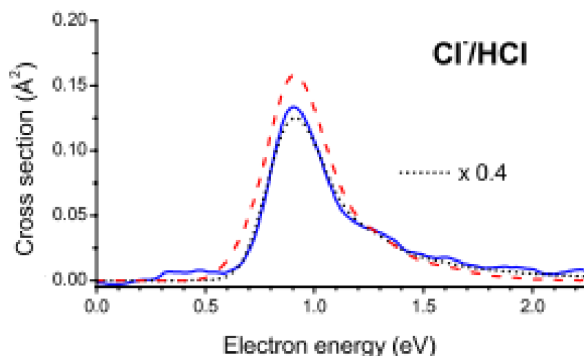


**Figure 4.6:** Dissociative electron attachment to HCl forming a  $\text{Cl}^-$  ion at  $\sim 1$  eV. The same contribution can be seen in the ion yield of  $\text{Cl}^-$  from  $\text{GeCl}_4$  in figure 4.5. Figure taken from reference 40

### 4.3.3 Ion yield in the range of 4-7 eV

A contribution from the high energy E resonance is observed in all four ion yields peaking at 5-6 eV, and as before, most likely stems from the same resonances as detected by electron transmission and in the total cross section spectra discussed in the text above. While  $\text{GeCl}_3^-$  formation dominates through the 0 eV resonance as the energetically favorable dissociation channel, different behavior is observed from contributions from the higher energy resonance

#### 4 Results And Discussion

at  $\sim 5$  eV. There the formation of  $\text{Cl}^-$  is the preferred pathway in spite of the higher electron affinity of  $\text{GeCl}_3^-$ . This could be the result of the extra electron and/or the excited electron being predominately located at the chlorine atom. Thus the dissociation pathway resulting in a  $\text{Cl}^-$  ion may become favorable.

In the ion yields of  $\text{GeCl}_2^-$  and  $\text{Cl}_2^-$ , the appearance energies of the contributions from the same resonance are shifted upwards by  $\sim 0.7$  eV with respect to  $\text{GeCl}_3^-$  and  $\text{Cl}^-$  (see figure 4.5 and table 4.1). The intensity of these fragments is also significantly lower than for the formation of  $\text{Cl}^-$  which requires only the rupture of a single bond. This indicates a potential barrier associated with the dissociation of two Ge—Cl bonds, causing the ions to appear only through the high energy flank of the resonance.

Interestingly, the dominance of the formation of a single halide ion through high energy resonances was also observed in DEA spectra of the  $\text{GeF}_4$ <sup>1</sup> and  $\text{GeBr}_4$ <sup>2</sup> congeners. Additionally, the shift to higher electron energies when two Ge—X bonds are ruptured, can also be noticed in those measurements.

## 5 Summary

This thesis study has presented DEA measurements on  $\text{GeCl}_4$  using a continuous crossed electron and molecular beam apparatus. The study is a part of a larger effort to document the low-energy electron interactions with group IV tetrahalides  $\text{XY}_4$  ( $\text{X} = \text{C}, \text{Si}, \text{Ge}$  and  $\text{Y} = \text{F}, \text{Cl}, \text{Br}$ ). Initially, the nature of negative ion formation through various resonances was examined along with subsequent relaxation pathways with focus on DEA. Fitting procedures for the determination of appearance energies were then discussed along with their limitations. Lastly, the measured ion yields of fragments formed by DEA to  $\text{GeCl}_4$  were presented and the nature of observed resonances discussed in context with previous studies on low-energy electron interaction with  $\text{GeCl}_4$ , where available.

The recorded fragments in the current measurements were  $\text{GeCl}_3^-$ ,  $\text{GeCl}_2^-$ ,  $\text{Cl}^-$  and  $\text{Cl}_2^-$  which appeared through three different resonances at 0, 1.4 and 5-6 eV, respectively. In earlier studies, these resonances have been observed and assigned symmetries in accordance with the incident electrons occupation of  $a_1$ ,  $t_2$  and  $e$  orbitals. The current measurements provide the first ion yields where all three resonances are detected in the same spectra. At 0 eV, the formation of  $\text{GeCl}_3^-$  dominates the ion yield due to the high electron affinity of  $\text{GeCl}_3^-$ , making it the energetically favorable pathway. However, through the higher energy resonance at 5-6 eV, the formation of  $\text{Cl}^-$  is the preferred pathway. This is most likely due to the increased electron density around the chlorine atom in the transient negative ion. The appearance energy of all contributions was determined by two individual fitting functions, providing good results in every case.

# List of Figures

1.1	MO diagram of $\text{GeCl}_4$ . . . . .	3
2.1	Born-Oppenheimer diagram explaining electron attachment and subsequent relaxation . . . . .	5
2.2	Schematic figure of resonant states . . . . .	7
2.3	Effective long-range interaction potential of an electron-molecule system .	8
3.1	SIGMA, the continuous crossed-beam electron attachment apparatus . . . .	10
3.2	Calibration of the energy signal using $\text{SF}_6^-$ and $\text{O}^-$ . . . . .	11
4.1	Dissociative Ionization spectrum of $\text{GeCl}_4$ . . . . .	14
4.2	Appearance energy determined by fits . . . . .	15
4.3	Wannier-type fitting limitations . . . . .	16
4.4	Linear fitting limitations . . . . .	16
4.5	DEA ion yield curves for $\text{GeCl}_4$ . . . . .	18
4.6	DEA spectra of $\text{HCl}$ . . . . .	21

# List of Tables

4.1	Appearance energy results . . . . .	17
-----	-------------------------------------	----

# Bibliography

- [1] **E. Bjarnason, F. Ómarsson, M. Hoshino, H. Tanaka, M. Brunger, P. Limão-Vieira and O. Ingólfsson.** *Negative ion formation through dissociative electron attachment to the group IV tetrafluorides: Carbon tetrafluoride, silicon tetrafluoride and germanium tetrafluoride.* International Journal of Mass Spectrometry, 339, (2013), 45.
- [2] **F. Ómarsson, B. Reynisson, M. Brunger, M. Hoshino, H. Tanaka, P. Limão-Vieira and O. Ingólfsson.** *Negative ion formation through dissociative electron attachment to the group IV tetrabromides: Carbon tetrabromide, silicon tetrabromide and germanium tetrabromide.* International Journal of Mass Spectrometry. In press. DOI=<http://dx.doi.org/10.1016/j.ijms.2014.01.008>.
- [3] **S. Sakaguchi and S. ichi Todoroki.** *Optical properties of GeO<sub>2</sub> glass and optical fibers.* Appl. Opt., 36 (27), (1997), 6809.
- [4] **Thiele and K. Ulrich.** *The Current Status of Catalysis and Catalyst Development for the Industrial Process of Poly(ethylene terephthalate) Polycondensation.* International Journal of Polymeric Materials, 50 (3-4), (2001), 387.
- [5] **R. Moskalyk.** *Review of germanium processing worldwide.* Minerals engineering, 17 (3), (2004), 393.
- [6] **F. Ahmed, S. Yunus, I. Kamal, S. Begum, A. Khan, M. Ahsan and A. Ahmad.** *Optimization of Germanium Monochromators for Neutron Diffractometers.* International Journal of Modern Physics E, 5, (1996), 131.
- [7] **R. Diehl, N. Prantzos and P. von Ballmoos.** *Astrophysical constraints from gamma-ray spectroscopy.* Nuclear Physics A, 777, (2006), 70.
- [8] **G. Laguzzi, L. Tommesani, L. Luvidi, R. Bucci and G. Brunoro.** *Thin layer activation technique application in bronze corrosion monitoring.* Corrosion science, 41 (1), (1999), 197.
- [9] **R. Pabst, J. Margrave and J. Franklin.** *Electron impact studies of the tetrachlorides and tetrabromides of silicon and germanium.* International Journal of Mass Spectrometry and Ion Physics, 25 (4), (1977), 361.
- [10] **F. Guillot, C. D  zarnaud-Dandine, M. Tronc, A. Modelli, A. Lisini, P. Decleva and G. Fronzoni.** *Empty levels in germanium compounds studied by XAS, ISEELS, ETS, DEAS and ab initio calculations: GeH<sub>4</sub>, GeCl and Ge(CH<sub>3</sub>)<sub>3</sub>Cl.* Chemical physics, 205 (3), (1996), 359.
- [11] **A. Modelli, M. Guerra, D. Jones, G. Distefano and M. Tronc.** *Low-energy electron capture in group 14 methyl chlorides and tetrachlorides: Electron transmission and dissociative electron attachment spectra and MS-X  calculations.* The Journal of chemical physics, 108 (21), (1998), 9004.
- [12] **C. Szmytkowski, P. Mozejko and G. Kasperski.** *Low-and intermediate-energy total electron scattering cross sections for SiH<sub>4</sub> and GeCl<sub>4</sub> molecules.* Journal of Physics B: Atomic, Molecular and Optical Physics, 30, (1997), 4363.

## BIBLIOGRAPHY

- [13] **D. L. Azevedo, M. H. Bettega, L. G. Ferreira and M. A. Lima.** *Scattering of low-energy electrons by  $TiCl_4$ ,  $GeCl_4$ ,  $SiCl_4$  and  $CCl_4$ : a comparison of elastic cross sections.* Journal of Physics B: Atomic, Molecular and Optical Physics, 33 (24), (2000), 5467.
- [14] **P. Możejko, B. Żywicka-Możejko and C. Szmytkowski.** *Elastic cross-section calculations for electron collisions with  $XY_4$  ( $X = Si, Ge$ ;  $Y = H, F, Cl, Br, I$ ) molecules.* Nuclear instruments and methods in physics research section b: beam interactions with materials and atoms, 196 (3), (2002), 245.
- [15] **J. M. Riveros.** *Probing the gas-phase ion chemistry of simple Ge systems.* International Journal of Mass Spectrometry, 221 (3), (2002), 177.
- [16] **I. Lambert, S. Mason, R. Tuckett and A. Hopkirk.** *Electronic emission spectroscopy of Group IV tetrachloro molecular ions.* The Journal of chemical physics, 89 (5), (1988), 2675.
- [17] **J. Moc, J. M. Rudziński and H. Ratajczak.** *Comparative study of the structures and energies of the  $SiX_3$ ,  $GeX_3$  and  $SnX_3$  series of radicals ( $X = H, F, Cl$ ).* Chemical physics, 159 (2), (1992), 197.
- [18] **B. H. Boo, J. K. Lee and N. Saito.** *Dissociative Multiple Photoionization of  $GeCl_4$ : The Ge (3d, 3p, 3s) and Cl (2p, 2s) Inner-Shell Excitation in the Range 88 - 1006 eV.* The Journal of Physical Chemistry A, 106 (8), (2002), 1511.
- [19] **J. Creasey, I. Lambert, R. Tuckett, K. Codling, L. Frasinski, P. Hatherly, M. Stankiewicz and D. Holland.** *Nonradiative decay pathways of electronic states of group IV tetrafluoro and tetrachloro molecular ions studied with synchrotron radiation.* The Journal of Chemical Physics, 93 (5), (1990), 3295.
- [20] **R. Egdell, I. Fragala and A. Orchard.** *He (II) photoelectron spectra of the Group IVB tetrachlorides.* Journal of Electron Spectroscopy and Related Phenomena, 17 (4), (1979), 267.
- [21] **J. Green, M. Green, P. J. Joachim, A. Orchard and D. Turner.** *A study of the bonding in the group IV tetrahalides by photoelectron spectroscopy.* Philosophical Transactions of the Royal Society of London. Series A, Mathematical and Physical Sciences, 268 (1184), (1970), 111.
- [22] **B. Ómarsson.** *Promoting reaction channels in dissociative electron attachment through bond formation and rearrangement.* Ph.D thesis, Faculty of Physical Sciences, University of Iceland, Reykjavík, Iceland, (2013).
- [23] **F. Ómarsson.** *Symmetries, dynamics and energetics in dissociative electron attachment to selected group IV halides.* Ph.D thesis, Faculty of Physical Sciences, University of Iceland, Reykjavík, Iceland, (2014).
- [24] **M. Allan.** *Study of triplet states and short-lived negative ions by means of electron impact spectroscopy.* Journal of Electron Spectroscopy and Related Phenomena, 48 (2), (1989), 219.
- [25] **G. J. Schulz.** *Resonances in electron impact on diatomic molecules.* Reviews of Modern Physics, 45 (3), (1973), 423.
- [26] **E. Bjarnason, B. Ómarsson, S. Engmann, F. Ómarsson and O. Ingólfsson.** *Dissociative electron attachment to titanium tetrachloride and titanium tetraisopropoxide.* Eur. Phys. J. D. (2014), DOI: 10.1140/epjd/e2014-50091-9.
- [27] **A. Stamatovic and G. Schulz.** *Trochoidal electron Monochromator.* Rev. Sci. Instrum., 39 (11), (1968), 1752.
- [28] **D. Klar, M.-W. Ruf and H. Hotop.** *Attachment of electrons to molecules at submillielectronvolt resolution.* Chemical physics letters, 189 (4), (1992), 448.

## BIBLIOGRAPHY

- [29] **G. Schulz.** *Cross Sections and Electron Affinity for  $O^-$  Ions From  $O_2$ ,  $CO$ , and  $CO_2$  by Electron Impact.* Physical review, 128 (1), (1962), 178.
- [30] **P. Cicman, G. Senn, G. Denifl, D. Muigg, J. Skalny, P. Lukac, A. Stamatovic and T. Märk.** *Dissociative electron attachment to  $CO_2$ .* Czechoslovak journal of physics, 48 (10), (1998), 1135.
- [31] **S. Matt, O. Echt, R. Wörgötter, V. Grill, P. Scheier, C. Lifshitz and T. Märk.** *Appearance and ionization energies of multiply-charged  $C_{70}$  parent ions produced by electron impact ionization.* Chemical physics letters, 264 (1), (1997), 149.
- [32] **S. Stein.** *Mass spectra of  $GeCl_4$ .* NIST Mass Spec Data Center, (2011). Taken from <http://webbook.nist.gov/cgi/cbook.cgi?ID=C10038989&Units=SI&Mask=200#Mass-Spec> on april 21. 2014.
- [33] **P. Burrow, A. Modelli, N. Chiu and K. Jordan.** *Temporary negative ions in the chloromethanes  $CHCl_2F$  and  $CCl_2F_2$ : Characterization of the  $\sigma^*$  orbitals.* The Journal of Chemical Physics, 77 (5), (1982), 2699.
- [34] **L. V. Gurvich and I. Veyts.** *Thermodynamic Properties of Individual Substances: Elements and Compounds*, volume 2. CRC Press, 1990.
- [35] **J. Bartness.** *Electron affinity of neutral species.* Negative Ion Energetics Data, NIST Chemistry webbook, (2011). Taken from <http://webbook.nist.gov/cgi/cbook.cgi?ID=B139&Mask=20#Ion-Energetics> on april 23. 2014.
- [36] **U. Berzinsh, M. Gustafsson, D. Hanstorp, A. Klinkmüller, U. Ljungblad and A.-M. Mårtensson-Pendrill.** *Isotope shift in the electron affinity of chlorine.* Physical Review A, 51 (1), (1995), 231.
- [37] **J. Bartness.** *Electron affinity of neutral species.* Negative Ion Energetics Data, NIST Chemistry webbook, (2011). Taken from <http://webbook.nist.gov/cgi/cbook.cgi?ID=B181&Units=SI&Mask=1#Thermo-Gas> on april 23. 2014.
- [38] **P. Samartzis, I. Sakellariou, T. Gougousi and T. Kitsopoulos.** *Photofragmentation study of  $Cl_2$  using ion imaging.* Journal of Chemical Physics, 107 (1), (1997), 43.
- [39] **K. Bowen, G. Liesegang, B. Sanders and D. Herschbach.** *Electron attachment to molecular clusters by collisional charge transfer.* The Journal of Physical Chemistry, 87 (4), (1983), 557.
- [40] **J. Fedor, O. May and M. Allan.** *Absolute cross sections for dissociative electron attachment to  $HCl$ ,  $HBr$ , and their deuterated analogs.* Physical Review A, 78 (3), (2008), 032701.